PROCEEDINGS OF SPIE

SPIEDigitalLibrary.org/conference-proceedings-of-spie

Extraordinary enhancement of the transverse magneto-optical Kerr effect with high-refractive-index nanostructures

Carvalho, William O., Moncada-Villa, E., Oliveira, Osvaldo, Mejía-Salazar, J. R.

William O. F. Carvalho, E. Moncada-Villa, Osvaldo N. Oliveira, J. R. Mejía-Salazar, "Extraordinary enhancement of the transverse magneto-optical Kerr effect with high-refractive-index nanostructures," Proc. SPIE 11802, Nanoengineering: Fabrication, Properties, Optics, Thin Films, and Devices XVIII, 118020Q (1 August 2021); doi: 10.1117/12.2593929

SPIE.

Event: SPIE Nanoscience + Engineering, 2021, San Diego, California, United States

Extraordinary enhancement of the transverse magneto-optical Kerr effect with high-refractive-index nanostructures

William O. F. Carvalho [a], E. Moncada-Villa[b], Osvaldo N. Oliveira Jr. [c], and J. R. Mejía-Salazar [a]

[a]National Institute of Telecommunications (Inatel), Av. João de Camargo, 510, Centro, Santa Rita do Sapucaí, MG, 37540-000, Brazil
[b]Escuela de Física, Universidad Pedagógica y Tecnológica de Colombia, Av. Central del Norte 39-115, Tunja, Colombia
[c]Instituto de Física de São Carlos, Universidade de São Paulo, CP 369, 13560-970, São Carlos, SP, Brazil

ABSTRACT

We present a new proposal for enhancing the transverse magneto-optical Kerr effect (TMOKE) in the transmission mode using dielectric magneto-optical (MO) ribs deposited on a high-refractive-index (HRI) slab. Our concept is based on the phase-matching condition between the MO grating and the slab to produce extraordinary TMOKE amplitudes, which are superior to the most successful plasmonic approaches, and at least one order of magnitude higher than using dielectric MO gratings. It is also significant that there was almost no loss in the structure proposed owing to the low level of losses from the constituent materials. These features can be exploited in sensing and biosensing, as we demonstrated by considering the nanostructure in a typical liquid medium.

Keywords: Gratings, High-refractive-index, Magneto-optic, TMOKE

1. INTRODUCTION

Magneto-optical (MO) effects are at the core of several applications in filters, sensors, modulators, routers, data storage and spintronic devices.[1–9] These applications are mostly based on the transverse MO Kerr effect (TMOKE), which is associated with the relative change of reflected/transmitted waves when a transverse magnetization (magnetic field) is flipped.[10–12] Unfortunately, the very weak MO activity in smooth films of conventional ferromagnetic materials hampers device applications.[13–16] Magnetoplasmonic nanostructures, i.e., photonic platforms combining metallic and magnetic properties at the nanoscale, have been exploited because of their enhanced magneto-optical activity,[13,17] but applications are still hindered by the inherent Ohmic losses from metal inclusions in the optical regime. Such losses can be overcome using low-loss dielectric ferromagnetic materials, especially all-dielectric MO gratings and metasurfaces which may yield enhanced TMOKE amplitudes in reflection and transmission modes.[18–20] Nevertheless, the corresponding TMOKE amplitudes are still considered low when compared with their magnetoplasmonic counterparts.

A recent work[21] demonstrated the possibility to use a MO dielectric grating placed on a high-refractive-index (HRI) dielectric slab waveguide to produce TMOKE amplitudes higher than previous proposals. More specifically, diffracted waves from dielectric gratings[22] were coupled with guided modes into the HRI film (placed below the grating) to resemble the waveguide-plasmon-polariton approach[15,23,24] for enhanced MO effects. Inspired by this latter concept, we design here a MO dielectric grating with ribs made of cerium-substituted yttrium iron garnet (Ce:YIG),[25–28] placed on an AlSb HRI slab surrounded by air and grown on a SiO_2 substrate. Figure 1(a) shows the structure which is compatible with III-V or Si-based semiconductors to enable straightforward

Further author information: (Send correspondence to W.O.F.C.)
W.O.F.C.: E-mail: william.carvalho@dtel.inatel.br

Nanoengineering: Fabrication, Properties, Optics, Thin Films, and Devices XVIII, edited by Balaji Panchapakesan, André-Jean Attias, Wounjhang Park, Proc. of SPIE Vol. 11802, 118020Q · © 2021 SPIE · CCC code: 0277-786X/21/$21 · doi: 10.1117/12.2593929

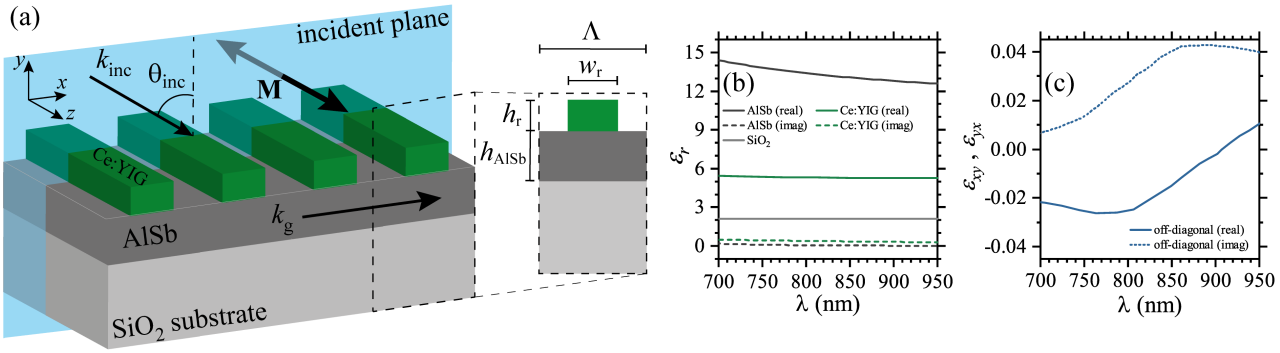

Figure 1. (a) Schematics of an all-dielectric system employed to enhance TMOKE. A Ce:YIG grating is deposited over an AlSb thin film on a SiO_2 substrate. The inset shows the geometric parameters employed. (b) Complex permittivities of the materials used and (c) off-diagonal permittivity of Ce:YIG for the magnetized system.

integration into on-chip MO applications. The materials selected can be grown via physical vapor deposition[26] or pulsed laser deposition.[27] The magnetization sense along the ribs-axes was used to control the resonant angle/wavelength of the grating and thus the corresponding coupling to the waveguide modes. We shall show that TMOKE amplitudes in the transmission mode can be around 15% in contrast with 10% from previous lossy plasmonic approaches.[15,29]

2. THEORY

TMOKE is a measure of the relative change in the transmission of obliquely incident p-polarized optical fields when the magnetization $\mathbf{M}$, oriented perpendicular to the incidence plane, is flipped[15]

$$\text{TMOKE} = 2\frac{T(+\mathbf{M}) - T(-\mathbf{M})}{T(+\mathbf{M}) + T(-\mathbf{M})}, \tag{1}$$

with $T(\pm\mathbf{M})$ indicating the transmittance for $\mathbf{M}$ pointing along the $\pm\hat{\mathbf{e}}_z$ direction, respectively, in Figure 1(a). The transmittance, TMOKE and near-fields were calculated using the finite element method (FEM) within the commercial software COMSOL Multiphysics®. Refined meshes were used for the whole structure for precision purposes. The Floquet periodic boundary conditions were used for the x-axis with perfect matched layers (PMLs) along the y-boundaries. Calculations were performed for wavelengths (λ) from 700 nm to 950 nm, and the incident angle (θ_{inc}) from $-25°$ to $90°$. Numerical sweeps were performed with steps of 0.1 nm and 0.05° for λ and θ_{inc}, respectively. The MO grating is considered as a one-dimensional periodic pattern along the x-axis (with period Λ), as illustrated in Figure 1(a), where w_{r} and h_{r} represent the width and height of the ribs. The length of the ribs (made of Ce:YIG) is infinite, with their axes placed along the z-axis. The HRI slab below the grating is made of AlSb III-V semiconductor with thickness h_{AlSb} and permittivity[30] $\varepsilon_{\text{AlSb}}$. The SiO_2 substrate is taken as semi-infinite, with permittivity[31] ε_{SiO_2}. The anisotropic permittivity $\varepsilon_{\text{Ce:YIG}}$ of MO Ce:YIG was taken as[25,28]

$$\tilde{\varepsilon}_{\text{Ce:YIG}} = \begin{pmatrix} \varepsilon_{\text{Ce:YIG}} & i\varepsilon_{xy}m & 0 \\ -i\varepsilon_{yx}m & \varepsilon_{\text{Ce:YIG}} & 0 \\ 0 & 0 & \varepsilon_{\text{Ce:YIG}} \end{pmatrix}, \tag{2}$$

where $\varepsilon_{\text{Ce:YIG}}$ and $\varepsilon_{xy} = \varepsilon_{yx}$ are the complex diagonal and off-diagonal values of the permittivity tensor. $m = +1$ ($m = -1$) is used to indicate that the magnetization is pointing along the positive (negative) z-axis. The permittivities are shown in Figures 1(b) and 1(c) as functions of the incident wavelength, for the diagonal and off-diagonal components, respectively.

3. RESULTS AND DISCUSSION

The nanostructure was optimized to work at $\lambda = 880$ nm since Ce:YIG has low levels of losses in the infrared, and a period length $\Lambda = 300$ nm, $w_{\text{r}} = 125$ nm, was used for the grating with $h_{\text{r}} = 80$ nm and $h_{\text{AlSb}} = 130$ nm.

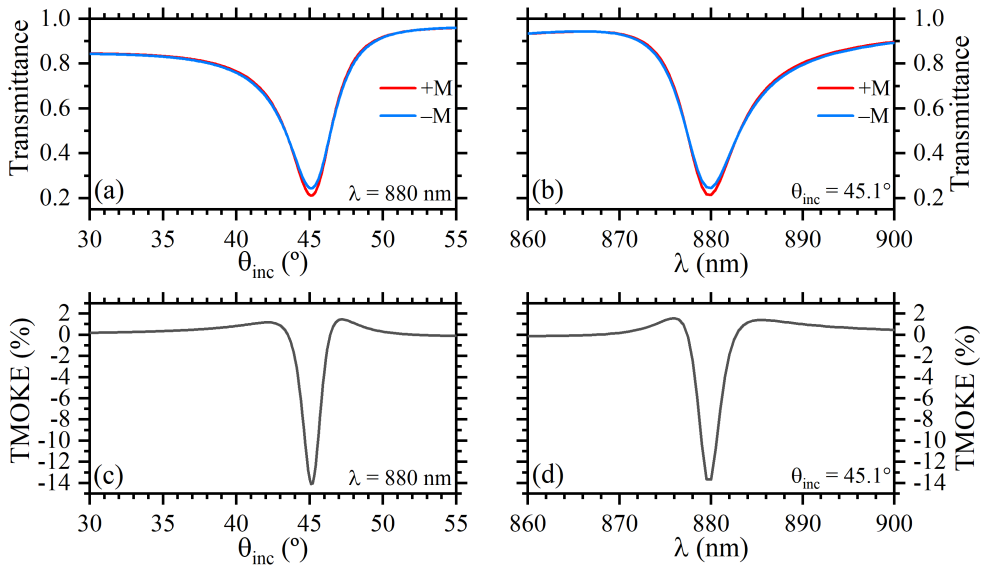

Figure 2. Transmittances T(+M), T(−M) for (a) $\lambda = 880$ nm as a function of θ_{inc} and (b) $\theta_{\text{inc}} = 45.1°$ as a function of λ. TMOKE curves (c) and (d) calculated using Eq. 1 for (a) and (b) cases, respectively. A strong Kerr effect of −14.09% was found in both cases.

The transmittances are presented as functions of the incident angle and wavelength in Figures 2(a) and 2(b), respectively. The minimum in the transmittance is explained in terms of waveguiding at the AlSb HRI, reached by resonant coupling through the phase-matching condition[20]

$$k_{\text{inc}} \sin(\theta_{\text{inc}}) + l\frac{2\pi}{\Lambda} = k_{g,\mathbf{M}}, \tag{3}$$

with k_{inc} and $k_{g,\mathbf{M}}$ indicating the wave vectors for the incident and guided modes, respectively. Subindices g and $\mathbf{M}$ are used to indicate that the guided modes not only depend on the periodicity of the grating (g) but also on the magnetization sense in the z-axis ($\mathbf{M}$). l is an integer number that denotes the diffraction order. The TMOKE amplitudes from the transmittance in Figures 2(a)-(b) are shown in Figure 2(c)-(d), respectively, where the amplitude modulation yields TMOKE values as high as 14% in both cases. The TMOKE U-shapes, instead of conventional Fano-like curves, were originated by the high off-diagonal values (high level of losses) for Ce:YIG at $\lambda = 880$ nm, as it can be seen in Figure 1(c). The dispersion equation for p-polarized modes can be obtained considering the alternating ribs as an effective MO medium. Then, the system in Figure 1 can be assumed as a 4-layer structure, which comprises (from the top layer): $i = 1$) air; $i = 2$) an effective MO slab; $i = 3$ top layer slab; $i = 4$) SiO_2 substrate. Therefore, the corresponding dispersion can be written as[21]

$$\tan(d_2 q_2) = \frac{\beta_2\beta_3(\beta_1+\beta_4) + \beta_2(\beta_3^2+\beta_1\beta_4)\tan(d_3 q_3)}{\beta_3(\beta_2^2+\beta_1\beta_4+\beta_1\gamma_2-\beta_4\gamma_2-\gamma_2^2) + (-\beta_1\beta_3^2-\beta_2^2\beta_4+\beta_3^2\gamma_2-\beta_1\beta_4\gamma_2+\beta_4\gamma_2^2)\tan(d_3 q_3)}, \tag{4}$$

where

$$\beta_i = \eta_{i,jj} q_i, q_i = \sqrt{\frac{\omega^2}{c^2}\frac{1}{\eta_{i,jj}} - k_x^2}, \tag{5}$$

with

$$\gamma_2 = -\frac{im\varepsilon_{xy}}{\varepsilon_{jj}-\varepsilon_{xy}^2} k_x \tag{6}$$

and

$$\eta_{i,jj} = \begin{cases} \frac{1}{\varepsilon_{i,jj}}, & i = 1,3,4 \\ \frac{\varepsilon_{i,jj}}{\varepsilon_{i,jj}^2-\varepsilon_{xy}^2}, & i = 2, \end{cases} \tag{7}$$

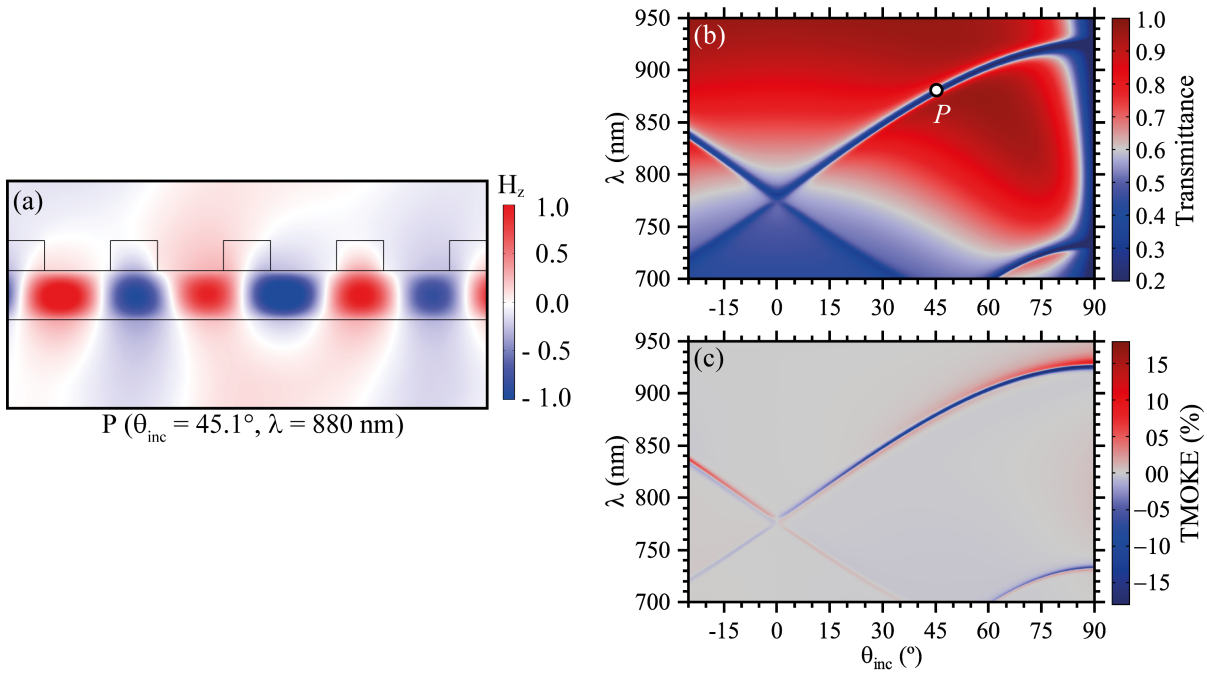

Figure 3. (a) H_z-field profile when the phase-match is satisfied for $\theta_{\text{inc}} = 45.1°$ and $\lambda = 880$ nm, named here as point P. Surface plot of (b) Transmittance T(+M) and (c) TMOKE. A large T is observed for $\lambda > 800$ nm up to an incident wave angle of 80°.

with subindex i indicating the corresponding layer material ($i = 1$ for air; $i = 2$ for the effective MO slab; $i = 3$ for the AlSb slab; $i = 4$ for the SiO_2 substrate) and $j = x, y, z$. For the grating structure, k_x is related to $k_{\text{g,M}}$ through Eq. (3), which indicates that the TMOKE enhancement comes from the control of the phase-matching between diffracted waves at the grating and guided modes in the HRI slab, in analogy to previous plasmonic mechanisms.[15]

The H_z-field coupled and guided in the AlSb slab is shown in Figure 3(a). For visualization purposes, we varied λ and θ_{inc} simultaneously in calculating the transmittance and the coupling regions, as well as the respective TMOKE values. Figures 3(b)-(c) show the results for $-25° \leq \theta_{\text{inc}} \leq 90°$ and 700 nm $\leq \lambda \leq$ 950 nm using the magnetized system in $\mathbf{M} = +1$. High transmittances are observed for $\lambda > 800$ nm [see dark red zone in Figure 3(b)], besides the well defined coupling region in blue, except for $\theta_{\text{inc}} > 80°$ which denotes high reflection due to larger incident angle and high absorbance for $\lambda < 800$ nm. TMOKE amplitudes up to 14% were obtained using Eq. 1, as observed from Figure 3(c).

In order to elucidate potential applications of this proposal in biosensing platforms, we used the incident medium with refractive index larger than 1.0 (used for air). Results were obtained for the incident refractive index varying from $n_{\text{a}} = 1.3$ to $n_{\text{a}} = 1.5$, which is consistent with refractive index changes in aqueous media for biosensing purposes.[32] The numerical data in Figure 4(a) shows that increasing of n_{a} induces a change in the resonant angle and TMOKE amplitudes. The sensing performance, defined by[2]

$$S(\theta_{\text{inc}}) = \left| \frac{\Delta\theta_{\text{res}}}{\Delta n_{\text{a}}} \right|, \tag{8}$$

is shown in Figure 4(b), where $\Delta\theta_{\text{res}}$ is the wavelength shift of the TMOKE peak associated with a change Δn_{a} in the refractive index of the analyte medium. $S(\theta_{\text{inc}})$ is given by °/RIU (refractive index unit). Figure 4(b) shows a linear behavior within the entire range of n_{a} values. Using a linear fitting, see the dashed line in Figure 4(b), we obtained a sensitivity of $S(\theta_{\text{inc}}) = 32.92°/\text{RIU}$, which is higher than recent plasmonic concepts.[12]

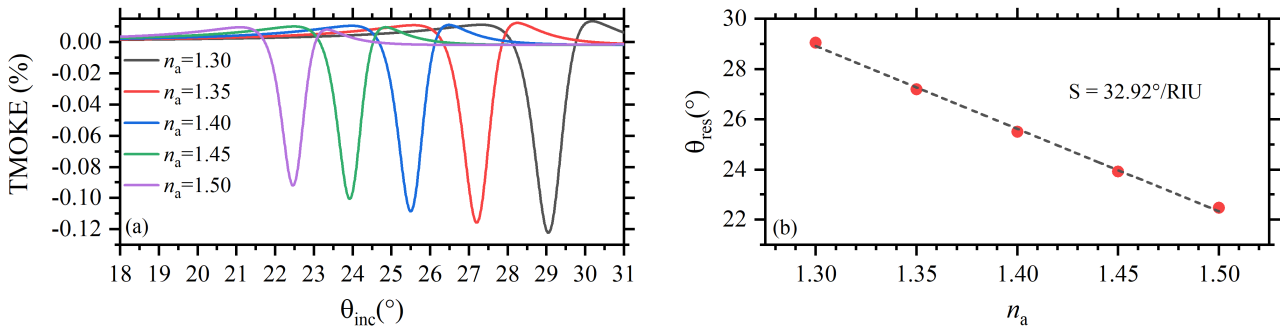

Figure 4. (a) H_z-field profile when the phase-match is satisfied for $\theta_{inc} = 45.1°$ and $\lambda = 880$ nm, named here as point P. Surface plot of (b) Transmittance T(+M) and (c) TMOKE. A large T is observed for $\lambda > 800$ nm up to an incident wave angle of 80°.

4. CONCLUSIONS

We have shown with theoretical simulations that MO dielectric gratings placed on a HRI slab can be used to produce enhanced TMOKE amplitudes. By changing the magnetization sense along the MO ribs we alter the resonant angle/wavelength, thus producing higher TMOKE amplitudes than in their magnetoplasmonic counterparts. Our proposal not only exhibits higher TMOKE amplitudes than magnetoplasmonic proposals but it also improves the efficiency through the use of low-loss dielectric materials. Significantly, we demonstrate that the structure proposed can be employed in sensing/biosensing applications.

ACKNOWLEDGMENTS

We acknowledge the financial support from the Brazilian agencies Coordenação de Aperfeiçoamento de Pessoal de Nível Superior - Brasil (CAPES) - Finance Code 001, National Council for Scientific and Technological Development-CNPq (429496/2018-4, 305958/2018-6), Research Support Foundation of Minas Gerais (FAPEMIG) and FAPESP (2018/22214-6). Partial financial support was also received from RNP, with resources from MCTIC, Grant No. 01245.010604/2020-14, under the 6G Mobile Communications Systems project of the Radiocommunication Reference Center (Centro de Referência em Radiocomunicações - CRR) of the National Institute of Telecommunications (Instituto Nacional de Telecomunicações - Inatel), Brazil.

REFERENCES

[1] Chau, K. J., Irvine, S. E., and Elezzabi, A. Y., "A gigahertz surface magneto-plasmon optical modulator," *IEEE J. Quantum Electron.* **40**, 571–579 (2004).

[2] Diaz-Valencia, B. F., Mejía-Salazar, J. R., Oliveira Jr, O. N., Porras-Montenegro, N., and Albella, P., "Enhanced transverse magneto-optical Kerr effect in magnetoplasmonic crystals for the design of highly sensitive plasmonic (bio) sensing platforms," *ACS Omega* **2**, 7682–7685 (2017).

[3] Huang, D., Pintus, P., Zhang, C., Morton, P., Shoji, Y., Mizumoto, T., and Bowers, J. E., "Dynamically reconfigurable integrated optical circulators," *Optica* **4**, 23–30 (2017).

[4] Ho, K.-S., Im, S.-J., Pae, J.-S., Ri, C.-S., Han, Y.-H., and Herrmann, J., "Switchable plasmonic routers controlled by external magnetic fields by using magneto-plasmonic waveguides," *Sci. Rep.* **8**, 10584 (2018).

[5] Borovkova, O. V., Hashim, H., Kozhaev, M. A., Dagesyan, S. A., Chakravarty, A., Levy, M., and Belotelov, V. I., "TMOKE as efficient tool for the magneto-optic analysis of ultra-thin magnetic films," *Appl. Phys. Lett.* **112**, 063101 (2018).

[6] Luo, L., Tang, T., Shen, J., and Li, C., "Electro-optic and magneto-optic modulations of Goos-Hänchen effect in double graphene coating waveguide with sensing applications," *J. Magn. Magn. Mater.* **491**, 165524 (2019).

[7] Gui, Q., Zhou, Y., Liao, S., He, Y., Tang, Y., and Wang, Y., "Inherently magnetic hydrogel for data storage based on the magneto-optical Kerr effect," *Soft Matter* **15**(3), 393–398 (2019).

[8] Dyakov, S. A., Fradkin, I. M., Gippius, N. A., Klompmaker, L., Spitzer, F., Yalcin, E., Akimov, I. A., Bayer, M., Yavsin, D. A., Pavlov, S. I., Pevtsov, A. B., Verbin, S. Y., and Tikhodeev, S. G., "Wide-band enhancement of the transverse magneto-optical Kerr effect in magnetite-based plasmonic crystals," *Phys. Rev. B* **100**, 214411 (2019).

[9] Oblak, E., Riego, P., Garcia-Manso, A., Martínez-de Guerenu, A., Arizti, F., Artetxe, I., and Berger, A., "Ultrasensitive transverse magneto-optical Kerr effect measurements using an effective ellipsometric detection scheme," *J. Phys. D: Appl. Phys.* **53**, 205001 (2020).

[10] Manera, M. G., Pellegrini, G., Lupo, P., Bello, V., de Julián Fernández, C., Casoli, F., Rella, S., Malitesta, C., Albertini, F., Mattei, G., and Rella, R., "Functional magneto-plasmonic biosensors transducers: Modelling and nanoscale analysis," *Sens. Actuators B Chem.* **239**, 100–112 (2017).

[11] Girón-Sedas, J. A., Gómez, F. R., Albella, P., Mejía-Salazar, J. R., and Oliveira Jr, O. N., "Giant enhancement of the transverse magneto-optical Kerr effect through the coupling of ε-near-zero and surface plasmon polariton modes," *Phys. Rev. B* **96**, 075415 (2017).

[12] Moncada-Villa, E., Oliveira Jr, O. N., and Mejía-Salazar, J. R., "ε-near-zero materials for highly miniaturizable magnetoplasmonic sensing devices," *J. Phys. Chem. C* **123**, 3790–3794 (2019).

[13] Belotelov, V. I., Akimov, I. A., Pohl, M., Kotov, V. A., Kasture, S., Vengurlekar, A. S., Gopal, A. V., Yakovlev, D. R., Zvezdin, A. K., and Bayer, M., "Enhanced magneto-optical effects in magnetoplasmonic crystals," *Nat. Nanotechnol.* **6**, 370 (2011).

[14] Armelles, G., Cebollada, A., García-Martín, A., and González, M. U., "Magnetoplasmonics: Combining magnetic and plasmonic functionalities," *Adv. Opt. Mater.* **1**, 10–35 (2013).

[15] Kreilkamp, L. E., Belotelov, V. I., Chin, J. Y., Neutzner, S., Dregely, D., Wehlus, T., Akimov, I. A., Bayer, M., Stritzker, B., and Giessen, H., "Waveguide-plasmon polaritons enhance transverse magneto-optical Kerr effect," *Phys. Rev. X* **3**, 041019 (2013).

[16] Kataja, M., Hakala, T. K., Julku, A., Huttunen, M. J., van Dijken, S., and Törmä, P., "Surface lattice resonances and magneto-optical response in magnetic nanoparticle arrays," *Nat. Commun.* **6**, 7072 (2015).

[17] Barsukova, M. G., Musorin, A. I., Shorokhov, A. S., and Fedyanin, A. A., "Enhanced magneto-optical effects in hybrid Ni-Si metasurfaces," *APL Photonics* **4**, 016102 (2019).

[18] Gamet, E., Varghese, B., Verrier, I., and Royer, F., "Enhancement of magneto-optical effects by a single 1D all dielectric resonant grating," *J. Phys. D: Appl. Phys.* **50**, 495105 (2017).

[19] Royer, F., Varghese, B., Gamet, E., Neveu, S., Jourlin, Y., and Jamon, D., "Enhancement of both Faraday and Kerr effects with an all-dielectric grating based on a magneto-optical nanocomposite material," *ACS Omega* **5**, 2886–2892 (2020).

[20] Voronov, A. A., Karki, D., Ignatyeva, D. O., Kozhaev, M. A., Levy, M., and Belotelov, V. I., "Magneto-optics of subwavelength all-dielectric gratings," *Opt. Express* **28**, 17988–17996 (2020).

[21] Carvalho, W. O. F., Moncada-Villa, E., Oliveira Jr, O. N., and Mejía-Salazar, J. R., "Beyond plasmonic enhancement of the transverse magneto-optical Kerr effect with low-loss high-refractive-index nanostructures," *Phys. Rev. B* **103**(7), 075412 (2021).

[22] Ko, Y. H. and Magnusson, R., "Wideband dielectric metamaterial reflectors: Mie scattering or leaky Bloch mode resonance?," *Optica* **5**, 289–294 (2018).

[23] Christ, A., Tikhodeev, S. G., Gippius, N. A., Kuhl, J., and Giessen, H., "Waveguide-plasmon polaritons: strong coupling of photonic and electronic resonances in a metallic photonic crystal slab," *Phys. Rev. Lett.* **91**, 183901 (2003).

[24] Kravets, V. G., Kabashin, A. V., Barnes, W. L., and Grigorenko, A. N., "Plasmonic surface lattice resonances: a review of properties and applications," *Chem. Rev.* **118**, 5912–5951 (2018).

[25] Onbasli, M. C., Beran, L., Zahradník, M., Kučera, M., Antoš, R., Mistrík, J., Dionne, G. F., Veis, M., and Ross, C. A., "Optical and magneto-optical behavior of cerium yttrium iron garnet thin films at wavelengths of 200–1770 nm," *Sci. Rep.* **6**, 23640 (2016).

[26] Bi, L., Hu, J., Jiang, P., Kim, H. S., Kim, D. H., Onbasli, M. C., Dionne, G. F., and Ross, C. A., "Magneto-optical thin films for on-chip monolithic integration of non-reciprocal photonic devices," *Materials* **6**, 5094–5117 (2013).

[27] Onbasli, M. C., Goto, T., Sun, X., Huynh, N., and Ross, C. A., "Integration of bulk-quality thin film magneto-optical cerium-doped yttrium iron garnet on silicon nitride photonic substrates," *Opt. Express* **22**, 25183–25192 (2014).

[28] Moncada-Villa, E. and Mejía-Salazar, J. R., "High-refractive-index materials for giant enhancement of the transverse magneto-optical Kerr effect," *Sensors* **20**, 952 (2020).

[29] Sadeghi, S. and Hamidi, S. M., "Bi:YIG@Au magneto-plasmonic core-shell nano-grating with robust, high magneto-optical figure of merit," *J. Magn. Magn. Mater.* **493**, 165709 (2020).

[30] Djurišić, A. B., Li, E. H., Rakić, D., and Majewski, M. L., "Modeling the optical properties of AlSb, GaSb, and InSb," *Appl. Phys. A* **70**, 29–32 (2000).

[31] Malitson, I. H., "Interspecimen comparison of the refractive index of fused silica," *J. Opt. Soc. Am. B* **55**, 1205–1209 (1965).

[32] Sreekanth, K. V., Alapan, Y., ElKabbash, M., Ilker, E., Hinczewski, M., Gurkan, U. A., De Luca, A., and Strangi, G., "Extreme sensitivity biosensing platform based on hyperbolic metamaterials," *Nat. Mater.* **15**(6), 621–627 (2016).